Planar B_4 Rhomboids: The Rare Earth Boride Halides $RE_4X_5B_4$†

Hj. Mattausch,*,‡ A. Simon, and C. Felser

Max-Planck-Institut für Festkörperforschung, Heisenbergstrasse 1, D-70569 Stuttgart, Germany

Received: May 2, 1997; In Final Form: June 30, 1997⊗

The new compounds $RE_4X_5B_4$ (RE = La, Ce, Pr, Gd and X = Br, I) and $RE_4I_5B_2C$ (RE = La, Ce) are prepared via the reaction of RE metal, REX_3 and B, or B and C at temperatures $1670 \geq T \geq 1270$ K in welded tantalum ampoules. Chains of interconnected B_4 rhomboids are the characteristic features of the crystal structures. According to band structure calculations, the compounds are one-dimensional metals which undergo a gradual metal-to-semiconductor transition at low temperature as experimentally indicated by the steep inrease of electrical resistivity.

Introduction

Rare earth metals exhibit a rich chemistry of borides as indicated by the general compositions REB_2, RE_2B_5, REB_4, REB_6, REB_{12}, and $REB_{\approx 66}$.[1,2] The structures are characterized by extended B−B bonding.

When the REB_x frameworks are fragmented as it is done in boride halides, interconnections between the B atoms are frequently lost, and one-dimensional, molecular or atomic boron entities result. The kind of entity is determined by a number of factors, e.g., size of the voids available and the number of electrons provided for B−B bonding by the RE−X framework, as well as by competition between RE−RE, B−B, and RE−B bonding, respectively. In the case of a sufficient surplus of metal valence electrons, the boride halides closely mimic the corresponding carbide halides as indicated by the existence of the isotypic pairs Gd_3Cl_3C/Gd_3Cl_3B,[3] Gd_4I_5C/Gd_4I_5B,[4] or $Sc_7Cl_{12}C/Sc_7Cl_{12}B$[5] which represent examples with three- and one-dimensionally condensed as well as discrete RE_6 octahedra, respectively, centered by interstitial B and C atoms. At reduced metal valence electron concentrations ($VEC/C_2 \leq 8$), the C_2 unit is the typical carbon species in rare earth carbide halides. In the case of mixed carbide boride halides, B−C bonding is frequently observed,[6] e.g., with the quasi molecular BC_2^{7-} anion, which is isoelectronic with SO_2.[7]

Here we report on boride halides and boride carbide halides with extended B−B bonding. The boride carbide halides $RE_4I_5B_2C$ exhibit an unusual structural separation of boron and carbon.

Results and Discussion

Projections of the crystal structures of $La_4I_5B_4$ and $La_4Br_5B_4$ are shown in Figures 1 and 2, respectively. The structure of $La_4I_5B_2C$ is depicted in Figure 3. All iodides $RE_4I_5B_4$, as well as $Pr_4Br_5B_4$, take the $La_4I_5B_4$ structure. $Ce_4Br_5B_4$ and $Ce_4I_5B_2C$ are isotypic with the corresponding La compounds.

The common motif in all three structures is the hitherto unknown linear chain of interconnected B_4 rhomboids embedded in channels of metal atoms, which are formed from RE octahedra. The channels are topologically related to those in the structure of $Gd_4I_5B_4$. As Figures 4a,b illustrate, the replacement of a single B atom in the center of the octahedron by a B_4 rhomboid essentially leads to an elongation of the shared octahedron edges from $d_{Gd-Gd} = 381$ to 472 pm, which is reflected in a characteristic change of the unit cell. Whereas the *a* and *b* axes are slightly different for $Gd_4I_5B_4$ (Gd_4I_5B), $a = 1850.8$ (1872.5) and $b = 426.0$ (406.7) pm, the *c* axes differ significantly, $c = 975.1$ (861.4) pm. The arrangement of the RE atoms around the B_4 rhomboids rather corresponds to

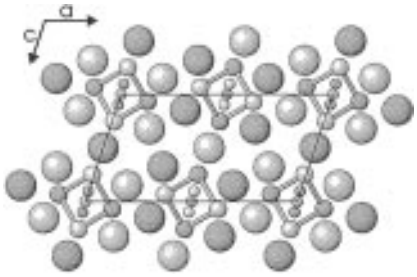

Figure 1. Projection of the structure of $La_4I_5B_4$ along [010]. The La bispenoids around the B_4 rhomboids are outlined (I, La, and B atoms with decreasing size).

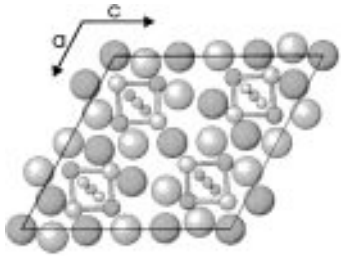

Figure 2. Projection of the structure of $La_4Br_5B_4$ along [010]. The La bispenoids around the B_4 rhomboids are outlined (Br, La, and B atoms with decreasing size).

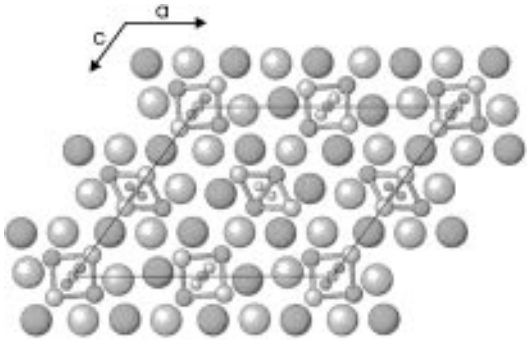

Figure 3. Projection of the structure of $La_4I_5B_2C$ along [010]. The La bispenoids around the B_4 rhomboids and the La octahedra around the C_2 pairs are outlined (I, La, B, and C atoms with decreasing size).

† Dedicated to Prof. Sir John Meurig Thomas on the occasion on his 65th birthday.

‡ Fax: International code + (711) 689-1642. E-mail: hansm@vaxff2.mpi-stuttgart.mpg.de.

⊗ Abstract published in *Advance ACS Abstracts,* November 1, 1997.

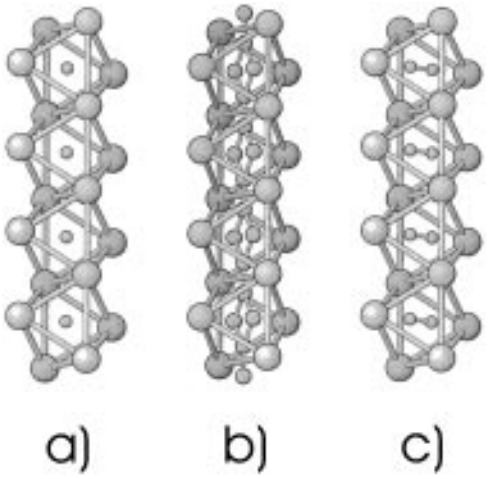

Figure 4. Characteristic building units in the RE boride−(carbide)−halides: chains of (a) RE_6 B octahedra, (b) RE_6B_4 octahedra (or rather bispenoids), and (c) RE_6C_2 octahedra.

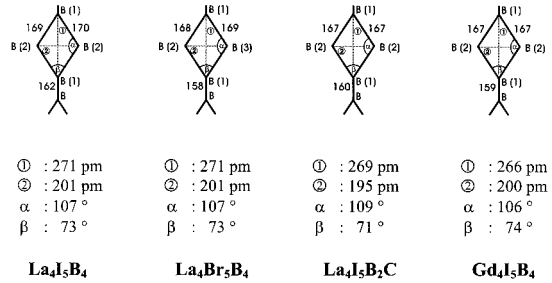

Figure 5. Distances and angles in and between the B_4 rhomboids in $RE_4X_5B_4$ and $La_4I_5B_2C$.

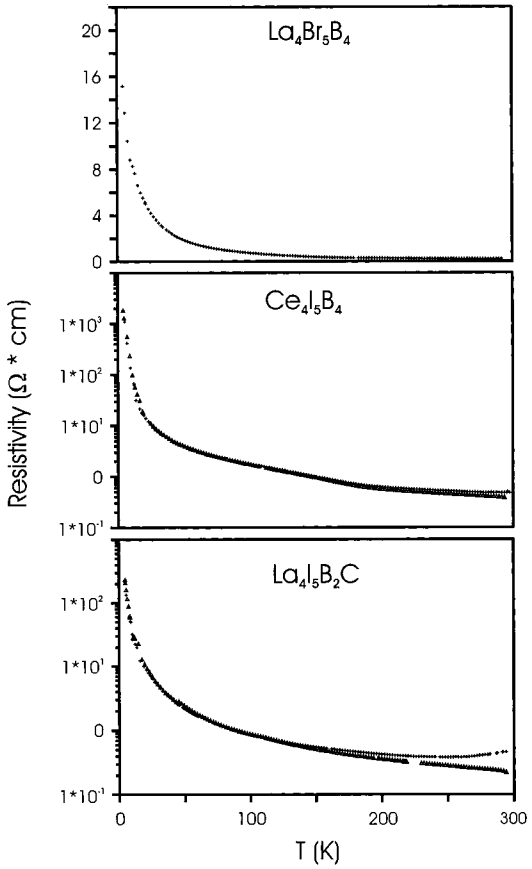

Figure 6. Electrical resistivity as a function of temperature of $La_4I_5B_4$, $Ce_4I_5B_4$, and $La_4I_5B_2C$ (crosses, heating curve, triangles, cooling curve).

channels of edge sharing bisphenoids. $La_4I_5B_4$ and $La_4Br_5B_4$ contain only such chains in a parallel arrangement, whereas in the structure of $La_4I_5B_2C$ these chains alternate layerwise with chains of C_2-centered RE octahedra as shown in Figure 4c. The one-dimensional RE−B and RE−C substructures are surrounded by halogen atoms. Assigning the X atoms above edges and apices of the RE polyhedra as X^i and X^a, respectively, the interconnection patterns of the structures can be rationalized according to Schäfer and Schnering:[8] $La_4I_5B_4$:$La_4I^i{}_2I^{i-i}{}_{2/2}I^{i-a}{}_{2/2}I^{a-i}{}_{2/2}B_4$, $La_4Br_5B_4$:$La_4Br^i{}_1Br^{i-i}{}_{3/2}Br^{i-a}{}_{3/2}Br^{a-i}{}_{2/2}B_4$ and $La_4I_5B_2C \equiv La_4I_5B_4 \cdot La_4I_5C_2$:$La_4I^i{}_2I^{i-i}{}_{2/2}I^{i-a}{}_{2/2}I^{a-i}{}_{2/2} \cdot La_4I^i{}_2I^{i-i}{}_{2/2}I^{i-a}{}_{2/2}I^{a-i}{}_{2/2}$.

The shortest B−X distances range for example from 380 to 400 pm ($La_4Br_5B_4$) and from 390 to 400 pm ($Gd_4Br_5B_4$), respectively.

The compound $La_4I_5B_2C$ is a most unusual intergrowth phase of $La_4I_5B_4$ and $La_4I_5C_2$,[9] (which are both known as dicrete compounds. Instead of B−C bonding as it normally occurs in boride carbides[10,11] and boride carbide halides[7] of the rare earth metals the elements, B and C are structurally separated in $La_4I_5B_2C$. The distance $d_{C-C} = 130.5$ pm is in the range of what is found for C_2^{4-} ions, although with quite a large uncertainty of the experimental value. The same uncertainty holds for the B−B distances; however, the boron substructure occurs rather identical even with respect to geometrical details in all of the investigated crystal structures. Distances and angles for the $^1_\infty B_4$ chains in different compounds are compared in Figure 5.

The B_4 rhomboid is hitherto unknown in molecules and solids. In B_4Cl_4, distorted tetrahedra ($d_{B-B} = 173$ and 170 pm) occur.[12] B_4H_{10} has the arachno-type butterfly arrangement ($d_{B-B} = 171$ pm).[13,14] The topology of the neutral $B_4(t\text{-Bu})_4$ is unknown, and it is only the radical ion $B_4(t\text{-Bu})_4^-$ which might have a planar B_4 fragment according to electron spin resonance measurements.[15] The B_4 fragment looks very similar in all investigated compounds, $RE_4X_5B_4$ and $La_4I_5B_2C$, respectively. The edge length is approximately 170 pm, and the distances across the rhomboid are 200 and 270 pm, respectively. The B_4 units are connected via short distances $d_{B-B} = 160$ pm to form linear chains.

The B−B distances can be analysed in terms of Pauling bond orders (PBOs), taking $d = d(1) - 60 \log n$ with the single bond distance $d(1) = 159$ pm from the $^3\Sigma_g$ ground state of the B_2 molecule.[16] The distances $d_{B-B} = 160$ and 170 pm correspond to PBOs $n \approx 1$ and $n \approx 0.65$. The B atoms involved in the single bond are left with a "valency" of 0.7 for B−RE bonding, the others with approximately 1.7. It is interesting to note that the B atoms, which interconnect the B_4 rhomboids, have the same bonding capability to their metal atom environment as do the atoms in the B_6 octahedron in the structure of Gd_2B_5.[17] According to these rather hand waving arguments, two electrons are involved in the bonding between B_4 rhomboids and approximately five for bonding in the individual B_4 units.

The odd number of electrons in the B_4 unit, which is closely linked to adjacent ones, would suggest the phases to be one-dimensional metals. At low temperatures, electronic localization due to a Peierls transition is expected.

Figure 6 shows the results of resistivity measurements for selected samples. One has to be very cautious not to overinterpret measurements on pressed powder pellets, particularly in the case of one-dimensional metals because grain boundary effects may overshadow all intrinsic properties. However, the experimental results seem to corroborate the above assumption. The examples exhibit good conductivity at room temperature, and below approximately 50 K a step increase of the resistivity indicates a gradual transition to insulating

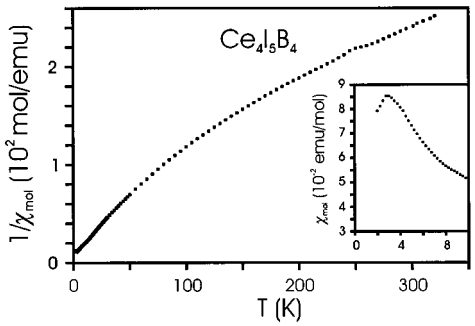

Figure 7. Reciprocal molar magnetic susceptibility of $Ce_4I_5B_4$ as a function of temperature at a magnetic field of 1 T. The inset shows the low-temperature part of the molar susceptibility with antiferromagnetic ordering at ≈3.5 K.

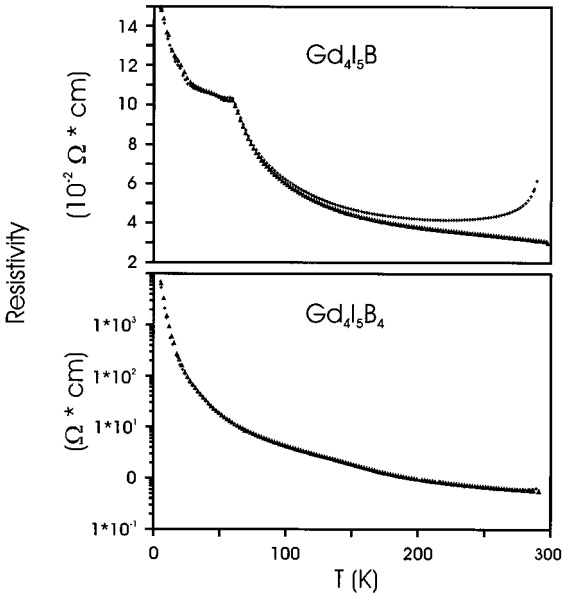

Figure 8. Comparison of the electrical resistivity as a function of temperature of Gd_4I_5B and $Gd_4I_5B_4$.

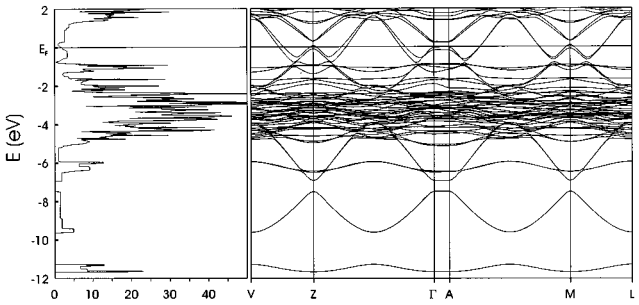

Figure 9. Left: The calculated total DOS of $La_4Br_5B_4$. The Fermi level E_F is the zero energy. Right: The band structure of $La_4Br_5B_4$ from −12 to 2 eV around the Fermi level.

behavior. Such smooth transition is well known from other compounds, e.g., MMo_3X_3 (M = Rb, Cs; X = Se, Te)[18] which is a one-dimensional metal at room temperature.

$La_4Br_5B_4$ is essentially nonmagnetic. The measured sample contains a magnetic impurity of less than 0.1% of a spin $^1/_2$ system. The magnetic properties of $Ce_4I_5B_4$ (Figure 7) show the cerium to be in the oxidation state +3 as expected (μ_{eff} = 2.4μ_B; expected value 2.5μ_B). The compound orders antiferromagnetically at 3 K.

It is interesting to note the dramatic differences between the corresponding physical properties of Gd_4I_5B, whose structure is characterized by single B atoms, Gd−Gd bonding, and short Gd−Gd distance, respectively, and $Gd_4I_5B_4$ with no Gd−Gd

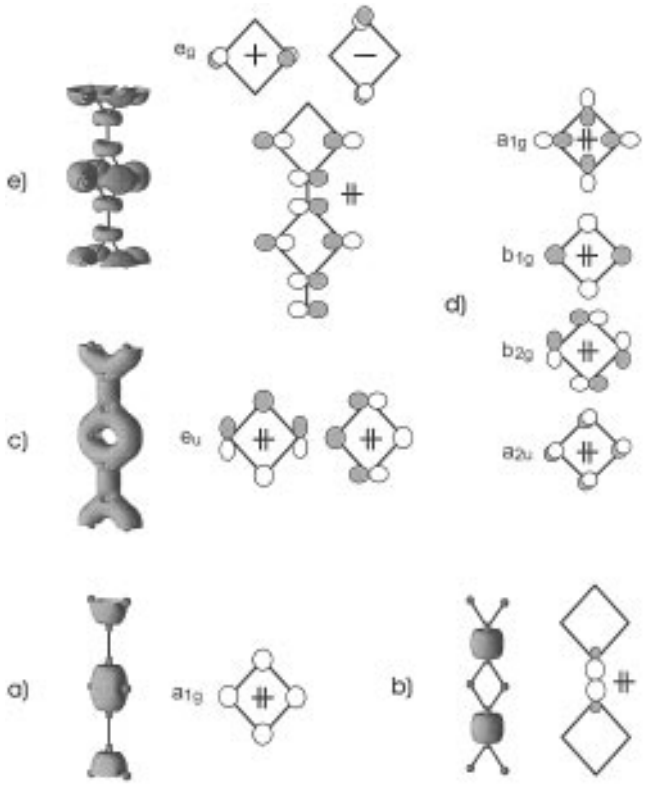

Figure 10. The MO diagram (without s−p mixing) of the idealized square planar B_4 unit together with the corresponding integrated LMTO-electron density. (a) The a_{1g} orbital and the electron density (0.2 e/a_o^3) well localized within the B_4 unit. (b) The MO and the electron density (0.2 e/a_o^3) between two different B_4 units (B(1)−B(1)). (c) The e_u orbital and the electron density (0.2 e/a_o^3) distributed both between neighboring B_4 units as well as in the periphery of one unit. (d) The a_{2u}, b_{2g}, b_{1g}, and a_{1g} MO's contributing to the bands above −5.5 eV (compare Figure 9 (right)). (e) The e_g MO (HOMO) and an additional MO below E_F. The electron density (0.2 e/a_o^3) has lone-pair character at B(2) and B(3), also the π interaction between B(1) and B(1) is very weak.

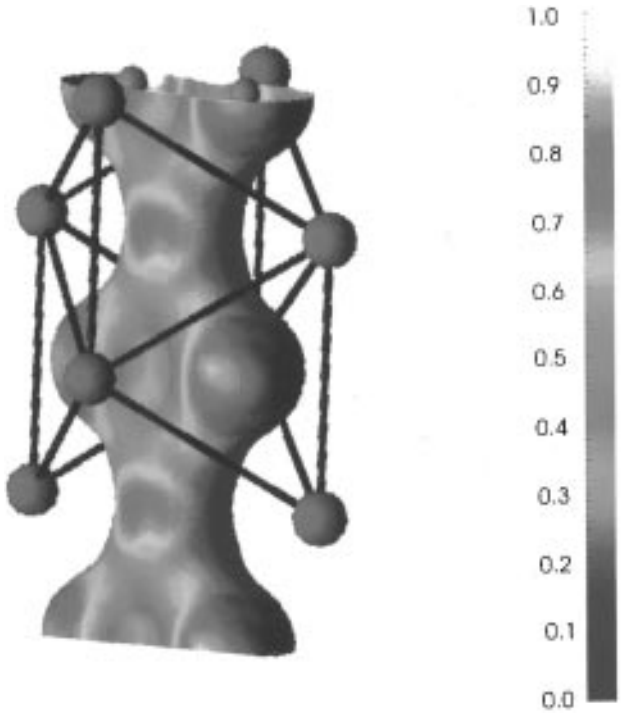

Figure 11. The isosurface of the total electron density (0.6 e/a_o^3) calculated within the concept of ELF. High localization: white; low localization, blue.

TABLE 1: Preparation of the Compounds $RE_4X_5B_4$

compound	educts	reacn temp (K)	time (*d*)	product
$La_4I_5B_4$	$5LaI_3$, 7La, 12B	1370	10	$La_4I_5B_4$ (100%)
$Ce_4I_5B_4$	$5CeI_3$, 7Ce, 12B	1340	5	$Ce_4I_5B_4$ (100%)
$Pr_4I_5B_4$	$5PrI_3$, 7Pr, 12B	1420	6	$Pr_4I_5B_4$ (90%)
$Nd_4I_5B_4$	$5NdI_3$, 7Nd, 12B	1320	5	$Nd_4I_5B_4$ (100%)
$Gd_4I_5B_4$	$5GdI_3$, 7Gd, 12B	1420	5	$Gd_4I_5B_4$ (80%)
$La_4Br_5B_4$	$5LaBr_3$, 7La, 12B	1450	7	$La_4Br_5B_4$ (100%)
$Ce_4Br_5B_4$	$5CeBr_3$, 7Ce, 12B	1420	5	$Ce_4Br_5B_4$ (100%)
$Pr_4Br_5B_4$	$5PrBr_3$, 7Pr, 12B	1270	5	$Pr_4Br_5B_4$ (50%)
$La_4I_5B_2C$	$1La_4I_5C_2$, $1La_4I_5B_4$	1670	1	$La_4I_5B_2C$ (90%)
$Ce_4I_5B_2C$	$5CeI_3$, 7Ce, 6B, 3C	1460	10	$Ce_4I_5B_2C$ (80%)

TABLE 2: Lattice Constants of the Compounds $RE_4X_5B_4$

compound	*a* (pm)	*b* (pm)	*c* (pm)	β(deg)
$La_4I_5B_4$	1924.2(4)	434.6(1)	1027.6(1)	108.21(1)
$Ce_4I_5B_4$	1903.3(2)	432.4(2)	1013.5(2)	107.77(1)
$Pr_4I_5B_4$	1889.6(4)	431.4(1)	1003.9(2)	107.39(2)
$Nd_4I_5B_4$	1883.1(3)	429.97(4)	997.8(1)	107.18(2)
$Gd_4I_5B_4$	1850.8(3)	426.04(6)	975.1(2)	106.38(2)
$La_4Br_5B_4$	1825.6(1)	429.4(3)	1925.3(7)	118.07(2)
$Ce_4Br_5B_4$	1806.2(4)	428.3(1)	1918.3(5)	118.48(2)
$Pr_4Br_5B_4$	1790.7(2)	427.3(2)	960.0(1)	111.87(1)
$La_4I_5B_2C$	2330.3(9)	429.9(1)	1899.1(4)	126.22(2)
$Ce_4I_5B_2C$	2319.4(5)	429.0(1)	1882.2(4)	126.50(1)

bonding or long Gd−Gd distance, respectively. The resistivity of Gd_4I_5B is much lower than that of $Gd_4I_5B_4$ (Figure 8), and the discontinuity at approximately 60K due to antiferromagnetic ordering indicates the enhancement of magnetic interaction due to metal−metal bonding along the short octahedron edge. The results for Gd_4I_5B are important to understand the bonding in the boride carbide halide $La_4I_5B_2C \equiv La_4I_5B_4 \cdot La_4I_5C_2$ in terms of B−B, C−C, and La−La bondings occuring simultaneously. All relevant interatomic distances in the $La_4I_5B_4$ part of $La_4I_5B_4 \cdot La_4I_5C_2$ are essentially the same as in the compound $La_4I_5B_4$ itself. Hence, no significant charge transfer is expected to occur between the boron and the carbon containing substructures. The C−C distance of 130 pm closely corresponds to that of a double bond, and the $La_4I_5C_2$ substructure has to be formulated as $(La^{3+}{}_4I^-{}_5C_2{}^{4-} \cdot 3e^-)$. Obviously, the excess of the metal valence electrons populates metal−metal bonding band states as in the case of Ce_4I_5B as well as in the compound $La_4I_5C_2$[9] where the La−La bonding states lie well below the Fermi level. In fact, the bonding is closely related to that in the prototype of all metal−metal-bonded rare earth compounds, $Gd_2Cl_3 = Gd^{3+}{}_2Cl^-{}_3 \cdot 3e^-$,[19−21] which is also a semiconductor.[22−24]

The results of band structure calculations on $La_4Br_5B_4$ are in agreement with the qualitative arguments on chemical bonding in this compound and with the measured electrical properties. Figure 9 shows the total density of states (DOS), together with the band dispersions. All bands are at least 2-fold degenerate because of the presence of two formula units in the primitive cell. Below −5 eV, only s and p states of boron contribute to the DOS. Between −5 and −2 eV, bands with mainly Br p and B p, mixed with La d character, occur, and around the Fermi

TABLE 3: Crystal Data, Data Collection, and Structure Determination

empirical formula	$La_4Br_5B_4$	$La_4I_5B_4$	$Gd_4I_5B_4$	$La_4I_5B_2C$
formula weight	998.43 [amu]	1233.38 [amu]	1306.74 [amu]	1223.77 [amu]
temperature	293 K	293 K (143 K)	293 K	293 K
crystal system	monoclinic	monoclinic	monoclinic	monoclinic
space group	$C2/m-C^3_{2h}$ (No.12)	$C2/m-C^3_{2h}$ (No.12)	$C2/m-C^3_{2h}$ (No.12)	$C2/m-C^3_{2h}$ (No.12)
unit-cell dimension	$a = 1825.59(12)$, $b = 429.42(3)$, $c = 1925.3(7)$pm, $\beta = 118.07(2)°$	$a = 1924.6(4)$, $b = 434.2(1)$, $c = 1028.3(2)$pm, $\beta = 108.28(3)°$ ($a = 1919.6(4)$, $b = 434.2(1)$, $c = 1026.5(2)$ pm, $\beta = 108.17(3)°$)	$a = 1848.8(4)$, $b = 425.7(1)$, $c = 974.0(2)$pm, $\beta = 106.40(3)°$	$a = 2330.3(9)$, $b = 429.9(1)$, $c = 1899.1(4)$pm, $\beta = 126.22(2)°$
volume	1.3317(5) nm^3	0.8159(3) nm^3 (0.8129(3) nm^3)	0.7354(3) nm^3	1.5349(8) nm^3
Z	4	2	2	4
density (calculated)	4.980 mg m^{-3}	5.020 mg m^{-3} (5.039 mg m^{-3})	5.901 mg m^{-3}	5.296 mg m^{-3}
absorption coefficient	14.636 mm^{-1} (Ag Kα)	19.677 mm^{-1} (Mo Kα)	15.053 mm^{-1} (Ag Kα)	11.057 mm^{-1} (Ag Kα)
color, habit	bluish-green, needles	bluish-green, needles	bluish-green, needles	black, needles
F(000)	1692	1026	1082	2036
crystal dimension	0.02 × 0.2 × 0.02 mm	0.03 × 0.2 × 0.02 mm	0.05 × 0.1 × 0.05 mm	0.05 × 0.2 × 0.05 mm
data collection	CAD4 (Nonius) Plane graphite monochromator λ(Ag Kα) = 56.086 pm ω scan, $\Delta\omega = 0.9°$ $4.00° \le 2\vartheta \le 52.00°$ $0 \le h \le 28$, $0 \le k \le 6$, $-30 \le l \le 26$	IPDS (Stoe) Plane graphite monochromator λ(Mo Kα) = 71.073 pm Detector distance 50,120 mm $7.00° \le 2\vartheta \le 56°$ $-26 \le h \le 26$, $-5 \le k \le 5$, $-14 \le l \le 10$	CAD4 (Nonius) Plane graphite monochromator λ(Ag Kα) = 56.086 pm ω/ϑ scan, $\Delta\omega = 1.0°$ $4.00° \le 2\vartheta \le 48.00°$ $0 \le h \le 24$, $-6 \le k \le 6$, $-14 \le l \le 13$	CAD4 (Nonius) Plane graphite monochromator λ(Ag Kα) = 56.086 pm ω/ϑ scan, $\Delta\omega = 0.9°$ $4.00° \le 2\vartheta \le 48.00°$ $-33 \le h \le 0$, $0 \le k \le 6$, $-22 \le l \le 27$
reflections collected	3012	2726 (2754)	2341	2569
independent reflections	2941 ($R_{int} = 0.052$)	993 ($R_{int} = 0.028$) (992 ($R_{int} = 0.034$))	1315 ($R_{int} = 0.030$)	2503 ($R_{int} = 0.019$)
structure refinement	FMLS on F^2 [30]	FMLS on F^2 [30]	FMLS on F^2 [30]	FMLS on F^2 [30]
absorption correction	empirical, ψ scans (15 reflections, $\mu r = 0.05$, 0.86 ≤ transmission ≤ 0.98)	none	empirical, ψ scans (9 reflections, $\mu r = 0.10$, 0.69 ≤ transmission ≤ 0.87)	empirical, ψ scans (8 reflections, $\mu r = 0.32$, 0.70 ≤ transmission ≤ 0.90)
data/restraints/parameters	2854/0/79	991/0/43 (985/0/43)	1315 / 0 / 43	2503 / 0 / 73
goodness of fit on F^2	1.260	1.038 (1.055)	1.159	1.103
final R indices [$I \ge 2\sigma(I)$]	$R1 = 0.0411$, $wR2 = 0.0642$	$R1 = 0.0232$, $wR2 = 0.0417$ ($R1 = 0.0248$, $wR2 = 0.0477$)	$R1 = 0.0187$, $wR2 = 0.0403$	$R1 = 0.0579$, $wR2 = 0.1051$
R indices [all data]	$R1 = 0.0643$, $wR2 = 0.0787$	$R1 = 0.0382$, $wR2 = 0.0450$ ($R1 = 0.0360$, $wR2 = 0.0514$)	$R1 = 0.0241$, $wR2 = 0.0428$	$R1 = 0.0642$, $wR2 = 0.1082$
largest max/min	2141/−1982 e nm^{-3}	1031/−929 e nm^{-3} (1031 / −1151 e nm^{-3})	2153 and −1028 e nm^{-3}	8340 and −11772 e nm^{-3}

TABLE 4: Atomic Coordinates, Equivalent U_{eq} and Anisotropic Displacement Coefficients U_{ij} (pm^2)[a]

atom	*x*	*y*	*z*	U_{eq}	U_{11}	U_{22}	U_{33}	U_{23}	U_{13}	*U*12
(a) $La_4I_5B_4$ at 293 (and 143 K), for All Atoms $U_{23} = U_{12} = 0$										
La(1)	0.1370(1)	0	0.0686(1)	139(1)	127(2)	131(2)	166(3)		58(2)	
(La(1)	0.1375(1)	0	0.0682(1)	75(1))	77(2)	69(2)	87(3)		37(2))	
La(2)	0.5101(1)	0	0.2538(1)	117(1)	169(2)	92(2)	107(3)		65(2)	
(La(2)	0.5114(1)	0	0.2547(1)	66(1))	94(2)	54(2)	57(3)		35(2))	
I(1)	0.3287(1)	0	0.1498(1)	190(2)	162(2)	186(3)	249(4)		101(2)	
(I(1)	0.3294(1)	0	0.1503(1)	96(1))	90(2)	98(3)	114(3)		52(2))	
I(2)	0.6879(1)	0	0.3218(1)	206(2)	198(3)	187(3)	203(3)		19(2)	
(I(2)	0.6895(1)	0	0.3217(1)	101(2))	99(3)	95(3)	99(3)		16(2))	
I(3)	0.5143(2)	$^1/_2$	0.5098(6)	352(9)	810(3)	136(5)	190(2)		260(2)	
(I(3)	0.5097(5)	$^1/_2$	0.5066(16)	202(13))	460(4)	79(5)	120(2)		170(4))	
B(1)	$^1/_2$	0.1803(18)	0	100(20)	150(30)	20(40)	130(40)		40(30)	
(B(1)	$^1/_2$	0.1862(22)	0	90(20))	110(40)	100(50)	70(40)		30(30))	
B(2)	0.9964(4)	0	0.9021(10)	140(20)	180(40)	70(40)	160(50)		30(40)	
(B(2)	0.9960(5)	0	0.9014(11)	90(20))	200(50)	20(40)	60(50)		20(40))	
(b) $La_4Br_5B_4$ at 293 K										
La(1)	0.1622(1)	$^1/_2$	0.2749(1)	119(1)	110(2)	108(2)	157(2)	0	76(2)	0
La(2)	0.3755(1)	0	0.3749(1)	103(1)	105(2)	83(2)	93(2)	0	24(2)	0
La(3)	0.3858(1)	$^1/_2$	0.1975(1)	116(1)	108(2)	114(2)	137(2)	0	67(2)	0
La(4)	0.1588(1)	0	0.0829(1)	118(1)	119(2)	102(2)	101(2)	0	26(2)	0
Br(1)	0.2242(1)	0	0.4052(1)	189(2)	251(5)	175(5)	185(4)	0	139(4)	0
Br(2)	0.0426(1)	0	0.1674(1)	155(2)	122(4)	165(4)	180(4)	0	72(3)	0
Br(3)	0.3340(1)	0	0.0661(1)	179(2)	204(4)	168(5)	156(4)	0	78(3)	0
Br(4)	0.0069(1)	$^1/_2$	0.3147(1)	169(2)	130(4)	180(5)	216(4)	0	96(3)	0
Br(5)	0	0	$^1/_2$	349(4)	372(9)	143(7)	220(7)	0	−119(6)	0
Br(6)	$^1/_2$	0	0	199(3)	171(6)	214(7)	175(6)	0	52(5)	0
B(1)	0.2693(4)	0.1843(16)	0.2285(4)	108(110)	120(20)	70(20)	110(20)	10(20)	40(20)	10(20)
B(2)	0.2268(5)	$^1/_2$	0.1725(6)	90(20)	40(30)	80(40)	140(40)	0	30(30)	0
B(3)	0.3119(6)	$^1/_2$	0.2866(6)	140(20)	110(40)	60(40)	170(40)	0	0(30)	0
(c) $Gd_4I_5B_4$ at 293 K, for All Atoms $U_{23} = U_{12} = 0$										
Gd(1)	0.1329(1)	0	0.0673(1)	117(1)	124(1)	102(1)	132(1)		45(1)	
Gd(2)	0.5059(1)	0	0.2498(1)	96(1)	151(1)	74(1)	72(1)		45(1)	
I(1)	0.3266(1)	0	0.1463(1)	160(1)	145(2)	148(2)	204(2)		80(1)	
I(2)	0.6821(1)	0	0.3186(1)	168(1)	168(2)	151(2)	161(2)		9(1)	
I(3)	0.5113(2)	$^1/_2$	0.5068(7)	278(7)	630(2)	118(3)	128(10)		170(2)	
B(1)	$^1/_2$	0.1871(15)	0	127(100)	190(20)	80(20)	110(20)		40(20)	
B(2)	0.9988(3)	0	0.8966(10)	89(90)	180(20)	30(20)	80(20)		80(20)	
(d) $La_4I_5B_2$ C at 293 K, for All Atoms $U_{23} = U_{12} = 0$										
La(1)	0.4874(1)	0	0.1250(1)	140(2)	195(4)	114(4)	144(4)		118(3)	
La(2)	0.4955(1)	0	0.4052(1)	358(3)	130(4)	744(10)	169(5)		71(4)	
La(3)	0.1325(1)	0	0.1050(1)	158(2)	163(4)	138(4)	167(4)		95(3)	
La(4)	0.1512(1)	0	0.6004(1)	441(4)	932(12)	187(5)	329(6)		440(8)	
I(1)	0.3215(1)	0	0.2529(1)	219(2)	182(5)	219(5)	178(5)		63(4)	
I(2)	0.3368(1)	0	0.7419(1)	240(2)	253(6)	229(6)	180(5)		96(4)	
I(3)	0.3164(1)	0	0.9782(1)	214(2)	200(5)	203(5)	282(5)		165(5)	
I(4)	0.0174(1)	0	0.7419(1)	410(4)	802(12)	254(7)	421(8)		498(9)	
I(5)	0.3355(1)	0	0. 5153(1)	250(3)	236(5)	227(6)	346(6)		206(5)	
C(1)	0.0343(16)	0	0.5231(19)	560(70)	870(190)	510(160)	610(170)		610(170)	
B(1)	$^1/_2$	0.1860(42)	0	150(30)	280(80)	100(70)	100(60)		130(60)	
B(2)	0.4968(8)	$^1/_2$	0. 0491(11)	120(30)	120(70)	30(60)	160(70)		60(60)	

[a] The U_{ij} are defined as $\exp[-2\pi^2(U_{11}h^2a^{*2} + ... + 2U_{23}klb^*c^*)]$.

level both B p and La d states contribute to the bands. The highly dispersive partly filled bands at E_F give evidence for the metallic nature of $La_4Br_5B_4$; a pseudogap is found 0.6 eV below the Fermi level. The one-dimensional character of $La_4Br_5B_4$ is obvious from the flat bands between Γ and A, which is the direction orthogonal to the B_4 chains. The Γ−A relates to the c axis. The Γ−Z and A−M run parallel to the chain direction.[25]

In order to reach a more quantitative interpretation of the electronic band structure, we refer to the MO diagram of the idealized square planar B_4 unit and in addition to the interaction between neighboring units as shown in Figure 10. Some of the orbital character is well preserved in discrete bands. The flat band having its bottom near −12 eV corresponds to the lowest a_{1g} orbital formed from the B s electrons. Integrating over all states through a suitably chosen energy window leads to the electron density which is plotted at a level of 0.2 e/a_o^3 in Figure 10a. It is obvious that the electron density is well localized within the B_4 unit, and there is no significant interaction between adjacent units. The (degenerate) band with its bottom near −10 eV does not contain a contribution from a B_4−MO, but the band is due to the interaction between neighboring B_4 units. Because this band is also energetically well separated from all other bands, the electron density can easily be evaluated. It is depicted in Figure 10b, again at a level of 0.2 e/a_o^3. The electron density is localized in the short bond between the B(1)-type atoms belonging to different B_4 units. The next sets of bands with their bottoms near −7 and −6.5 eV are derived from the e_u-type MO, which is degenerate in the case of a planar discrete B_4 unit. In the chain of interconnected rhomboids, two sets of doubly degenerate bands result. The one has s character at the B(1)-type atoms and exhibits large dispersion; the other is flat and corresponds to

TABLE 5: Selected Bond Lengths (pm) with Standard Deviation at 293 K

(a) $La_4I_5B_4$

La(1)	La(1): 434.2(1). La(2), 415.0(2), 422.3(2). I(1): 333.5(2), 351.8(3). I(2): 329.4(1). B(1): 286.5(4). B(2): 267.7(9) pm.
La(2)	La(2): 434.2(1). I(1): 331.5(2). I(2): 327.1(3). I(3): 339.4(5), 340.0(5). B(1): 267.3(3). B(2): 267.8(6) pm.
I(1)	I(1): 418.6(3), 434.2(1). I(2): 426.5(2). I(3): 441.1(4). B(1): 412.8(3). B(2): 417.8(8) pm.
I(2)	I(2): 428.5(2), 434.2(1). B(1): 413.9(3). B(2): 418.0(6) pm.
I(3)	I(3): 434.2(1). B(2): 415.5(12), 417.6(12) pm.
B(1)	B(1): 156.6(16), 277.6(16). B(2): 170.3(9) pm.
B(2)	B(2): 197.4(21) pm.

(b) $La_4Br_5B_4$

La(1)	La(1): 429.42(3). La(2): 405.31(9). La(4): 425.0(1). Br(1): 308.4(1). Br(2): 306.68(8). Br(4): 326.6(1). B(1): 284.7(8). B(2): 273.3(14).B(3): 263.5(12) pm.
La(2)	La(2): 429.42(3). La(3): 411.3(1). Br(1): 307.9(1). Br(4): 311.6(1). Br(5): 322.90(8). B(1): 268.0(6). B(3): 264.4(5) pm.
La(3)	La(3): 429.42(3). La(4): 424.8(1). Br(2): 317.7(1). Br(3): 310.6(1). Br(4): 314.58(9). B(1): 281.3(8). B(2): 271.0(10). B(3): 263.5(14) pm.
La(4)	La(4): 429.42(3). Br(2): 322.3(2). Br(3): 336.3(1). Br(6): 334.73(6). B(1): 269.0(6). B(2): 266.7(5) pm.
Br(1)	Br(1): 394.9(2), 429.42(3). Br(2): 420.3(2). Br(4): 411.0(1). B(1): 393.8(9). B(3): 397.8(12) pm.
Br(2)	Br(2): 429.42(3). Br(3): 399.1(1). Br(4): 385.0(2). Br(6): 363.9(1). B(1): 381.5(7). B(2): 395.1(9) pm.
Br(3)	Br(3): 362.7(2), 429.42(3). Br(4): 431.8(2). Br(6): 379.9(1). B(1): 390.8(9). B(2): 405.1(11) pm.
Br(4)	Br(4): 429.42(3). Br(5): 421.6(2). B(1): 392.6(7). B(3): 397.0(10) pm.
Br(5)	Br(5): 429.42(3). B(3): 392.4(9) pm.
Br(6)	Br(6): 429.42(3). B(2): 390.3(8) pm.
B(1)	B(1): 158.3(13), 271.2(13). B(2): 167.8(8). B(3): 169.5(8) pm.
B(2)	B(2): 200.6(13) pm.

(c) $Gd_4I_5B_4$

Gd(1)	Gd(1): 425.7(1). Gd(2): 394.5(1), 402.3(1). I(1): 320.9(1), 344.3(1). I(2): 317.7(1). B(1): 270.8(3). B(2): 255.7(5), 256.7(6) pm.
Gd(2)	Gd(2): 425.7(1). I(1): 318.1(1). I(2): 313.4(1). I(3): 326.6(5), 326.8(5). B(1): 253.3(2). B(2): 255.0(3) pm.
I(1)	I(1): 383.2(1), 425.7(1). I(2): 424.2(1). I(3): 449.7(5). B(1): 382.9(2). B(2): 392.6(5) pm.
I(2)	I(2): 425.7(1), 428.0(2). I(3): 459.6(5). B(1): 396.2(2). B(2): 401.8(4) pm.
I(3)	I(3): 425.7(1). B(2): 386.8(9), 388.1(9) pm.
B(1)	B(1): 159.3(13), 266.4(13). B(2): 166.6(6) pm.
B(2)	B(2): 200.2(12) pm.

(d) $La_4I_5B_2C$

La(1)	La(1): 429.9(1). La(3): 413.3(2), 420.9(2). I(2): 330.7(2). I(3): 324.5(2). I(4): 337.1(2). B(1): 268.0(6). B(2): 266.9(15) pm.
La(2)	La(2): 348.1(3), 429.9(1). La(4): 395.3(2), 398.6(3). I(1): 330.9(2). I(4): 339.4(2). I(5): 328.0(3). C(1): 284.1(23), 284.3(31) pm.
La(3)	La(3): 429.9(1). I(1): 355.8(2). I(2): 333.6(2). I(3): 327.9(2). B(1): 283.8(9). B(2): 268.6(13) pm.
La(4)	La(4): 429.9(1). I(1): 327.1(2). I(2): 349.2(3). I(5): 321.5(2). C(1): 219.5(33)pm.
I(1)	I(1): 429.9(1). I(2): 431.9(2). I(4): 418.8(2). I(4): 427.6(3). C(1): 413.3(22) pm.
I(2)	I(2): 429.9(1). I(5): 428.8(3). B(1): 413.5(4). B(2): 415.1(11) pm.
I(3)	I(3): 429.9(1). I(5): 428.8(3). B(1): 412.7(4). B(2): 417.3(18) pm.
I(4)	I(4): 429.9(1). I(5): 442.1(2). C(1): 440.0(45) pm.
I(5)	I(5): 429.9(1). C(1): 411.4(40) pm.
C(1)	C(1): 130.5(66) pm.
B(1)	B(1): 160.5(37), 269.4(37). B(2): 166.4(21) pm.
B(2)	B(2): 195.3(41) pm.

the configuration with p_x character at the B(1) type atoms. The electron density for the two sets of bands averaged over the entire Brillouin zone is shown at a level of 0.2 e/a_o^3 in Figure 10c. The electron density is distributed both between the B atoms of neighboring B_4 units as well as in the periphery of one unit itself. Last but not least the a_{2u}, b_{2g}, b_{1g}, and a_{1g} MOs contribute to the bands above −5.5 eV. These bands are strongly mixed with La d character; indeed, the latter dominates the band character. The e_g-type MOs split into highest occupied molecular orbital (HOMO) and lowest unoccupied molecular orbital (LUMO). Again covalent mixing with La d states adds to the dispersion of these bands. The HOMO is characterized by the node at the B(1) type atoms and p_z configuration at the other B atoms. The HOMO is half-occupied. It corresponds to the nearly degenerate band which crosses the Fermi level. The configuration depicted in the upper right of the Figure 10 leads to the flat bands around −1 eV. These bands contribute to the electron density which is depicted at a level of 0.1 e/a_o^3 in Figure 10e, indicating nonbonding interaction between all B atoms in these bands. The localization of nonbonding electron pairs at the B atoms is nicely demonstrated in Figure 11, which shows the isosurface of the total electron density at a level of 0.6 e/a_o^3. For the sake of clarity, the bromine atoms and the electron density related to these atoms is omitted. The degree of localization as it is calculated within the electron localization function (ELF) concept is shown by appropriate color of the isosurface. The region between the B(1)-type atoms, as well as positions at the other B atoms easily associated with lone pairs, are characterized by colors red to white indicating a large degree of localization.

Experimental Section

3.1. Preparation. Metals La, Ce, Pr, Nd, and Gd (sublimed, 99.99, Alfa/J. Matthey) were crushed directly with the exception of Gd which was hydrogenated, crushed, and dehydrogenated in vacuo at 1070 K (Mo container, 24 h). REX_3 was prepared from the oxides (99.9%, Alfa/J. Matthey), was with HX and NH_4X (p.a. Merck)[26,27] and distilled under vacuum in tantalum containers. Boron (99.4%, Ventron) and graphites (99.4%, Aldrich) were heated in vacuo at 1400 K for 12 h and 2 days, respectively, prior to use. Reactions were performed with stoichiometric mixtures of RE, REX_3, B, and C sealed in Ta capsules under Ar. Conditions are specified in Table 1. All boride halides exhibit a bluish-green metallic luster, and the boride carbide halides are black. The air and moisture sensitive products need to be handled in Ar.

3.2. X-ray Structure Investigation. The compounds are charactized by X-ray powder diffraction (modified Guinier

technique;[28] λ(Cu Kα_1) = 154.056 pm, internal standard Si, a = 543.035 pm, coincidence measurement). The lattice constants of all investigated compounds determined from powder data are summarized in Table 2. Single-crystal investigations were performed on selected compounds sealed in glass capillaries under Ar. Details on data collection and structure refinement are summarized in Table 3. The positions of the heavy atoms were derived by direct methods,[29] the light atoms were localized in ΔF maps. Full-matrix least-squares refinement[30] on F^2 led to the parameters shown in Table 4a for $La_4I_5B_4$ together with interatomic distances in Table 5a (Tables 4b and 5b for $La_4Br_5B_4$, Tables 4c and 5c for $Gd_4I_5B_4$ and Tables 4d and 5d for $La_4I_5B_2C$).[37]

The atoms I(3) ($La_4I_5B_4$ (293 and 143 K) and $Gd_4I_5B_4$ (293 K)) are temperature independently characterized by pronounced anisotropy of the displacement coefficients (U_{11}/U_{22}, $U_{33} \approx 15$). Occupation of a split position $x^1/_2z$ ($x \approx 0.510$, $z \approx 0.510$) instead of $^1/_2{}^1/_1{}^1/_2$ by this I(3) atom results in a "more isotropic" ratio U_{11}/U_{22}, $U_{33} \approx 5$ (Table 4a,c). Equivalent atoms in $La_4Br_5B_4$ (Br(5): U_{11}/U_{22}, $U_{33} \approx 2$) and in $La_4Br_5B_2C$ (I(4): U_{11}/U_{22}, $U_{33} \approx 3$) show similar anisotropy.

3.3. Electrical Conductivity. Measurements of the electrical conductivity were taken on pressed pellets (8 mm diameter) according to van der Pauw[31] at temperatures $4 \geq T \geq 300$ K in He atmosphere. All compounds $RE_4X_5B_4$ as well as $RE_4X_5B_2C$ exhibit metal-like resistivity at room temperature, and the resistivity increases strongly at low temperature. In the range $100 \geq T \geq 300$ K, the compounds seem to be small band gap semiconductors with gaps varying between the extremes E_g = 60 meV for $Gd_4I_5B_4$ and E_g = 10 meV for $La_4Br_5B_4$. Such assignment, however, is erroneous as both crystal and electronic band structures give evidence for one-dimensional metallic systems that gradually undergo localization.

3.4. Magnetic Susceptibility. Magnetic measurements in the range $2 \geq T \geq 300$ K were performed in a VTS-SQUID magnetometer (SHE) at a field of 1.0 T on samples (≈150 mg) enclosed in gelatine capsules.

3.5. Band Structure Calculations. Electronic band structures were calculated ab initio in the local density approximation within the TB-LMTO-ASA formalism.[32,33] Chemical bonding in $La_4Br_5B_4$ is visualized in real space as charge density and via the electron localization function ELF.[34] Calculations involve the La 6s, 5d, 4f, Br 4s, 4p and B 2s, 2p orbitals as basis sets. The La 6p, Br 4d and B 3d orbitals were treated in the socalled downfolding procedure. The exchange correlation potential is calculated according to,[35] and the band structure is based on 164 k points (tetrahedron method). The rather open structure needed the introduction of 98 empty spheres/primitive cell to meet the requirement of the atomic sphere approximation.

Acknowledgment. We thank R. Eger for experimental help, Dr. R. Pöttgen and H. Gärttling for the diffractometer measurements, and Dr. R. K. Kremer and E. Brücher for the electrical and magnetic measurements.

References and Notes

(1) *Gmelin Handbook RE Main*; Springer Verlag: Berlin, 1990; Vol. C 11a.
(2) Etourneau, J. *J. Less-Common Met.* **1985**, *110*, 267.
(3) Warkentin, E.; Simon, A. *Rev. Chim. Miner.* **1983**, *20*, 488.
(4) Simon, A.; Mattausch, Hj.; Miller, G. J.; Bauhofer, W.; Kremer, R. K. *Handbook on the Physics and Chemistry of Rare Earth*, Gschneidner, K. A., Jr, Eyring, L., Eds.; Elsevier Science Publishers: New York, 1991; Vol. 15, p 191.
(5) Dudis, D. S.; Corbett, J. D.; Hwu, S.-J. *Inorg. Chem.* **1986**, *25*, 3434.
(6) Mattausch, Hj.; Simon, A. *Angew. Chem.* **1995**, *107*, 1764; *Angew. Chem., Int. Ed. Engl.* **1995** *34*, 1633.
(7) Mattausch, Hj.; Simon, A.; Felser, C.; Dronskowski, R. *Angew. Chem.* **1996**, *108*, 1805; *Angew. Chem., Int. Ed. Engl.* **1996**, *35*, 1685.
(8) Schäfer, H.; Schnering, H. G. *Angew. Chem.* **1964**, *76*, 833; *Angew. Chem., Int. Ed. Engl.* **1964**, *3*, 3117.
(9) Mattausch, Hj. Unpublished results, 1993.
(10) Wiitkar, F.; Kahlal, S.; Halet, J.-F.; Saillard, J.-Y.; Bauer, J.; Rogl, P. *J. Am. Chem. Soc.* **1994**, *116*, 251.
(11) Ansel, D.; Bauer, J.; Bonhomme, F.; Boucekinne, G.; Frapper, G.;Halet, J.-F.; Gougeon, P. *Angew. Chem.* **1996**, *108*, 2245; *Angew. Chem., Int. Ed. Engl.* **1996**, *35*, 2098.
(12) Atoji, M.; Lipscomb, W. N. *Acta Crystallogr.* **1953**, *6*, 547.
(13) Nordman, C. E.; Lipscomb, W. N. *J. Chem. Phys.* **1953**, *21*, 1856.
(14) Moore, E. M.; Nordman, C. E.; Lipscomb, W. N. *J. Chem. Phys.* **1957**, *27*, 209.
(15) Klusik, H.; Berndt, A. *J. Organometal. Chem.* **1982**, *C17*, 234.
(16) Douglas, A. E.; Herzberg, G. *Phys. Rev.* **1940**, *57*, 752.
(17) Schwarz, C.; Simon, A. *Z. Naturforsch.* **1987**, *42b*, 935.
(18) Tarascon, J. M.; DiSalvo, F. J.; Waszczak, J. V. *Solid State Comm.* **1984**, *52*, 227.
(19) Mee, J. E.; Corbett, J. D. *Inorg. Chem.* **1965**, *4*, 88.
(20) Lokken, D. A.; Corbett, J. D. *Inorg. Chem.* **1973**, *12*, 556.
(21) Simon, A.; Holzer, N.; Mattausch, Hj. *Z. Anorg. Allg. Chem.* **1979**, *456*, 207.
(22) Bauhofer, W.; Simon, A. *Z. Naturforsch.* **1982**, *37a*, 568.
(23) Bullett, D. W. *Inorg. Chem.* **1980**, *19*, 1780.
(24) Bullett, D. W. *Inorg. Chem.* **1985**, *24*, 3319.
(25) Bradley, C. J.; Cracknell, A. P. *Theory of Symmetry in Solids*; Clarendon Press: Oxford, 1979.
(26) Brukl, A. *Angew. Chem.* **1939**, *52*, 152.
(27) Meyer, G.; Ax, P. *Mater. Res. Bull.* **1982**, *17*, 1447.
(28) Simon, A. *J. Appl. Crystallogr.* **1970**, *3*, 11.
(29) Sheldrick, G. M. *SHELXTL-PLUS, An Integrated System for Solving, Refining and Displaying Crystal Structures from Diffraction Data*; Göttingen: Germany, 1994.
(30) Sheldrick, G. M. *SHELXL-93*; Göttingen, Germany, 1993.
(31) van der Pauw, L. J. *Philips Res. Rep.* **1958**, *13*, 1.
(32) Krier, G.; Jepsen, O.; Burkhardt, A.; Andersen, O. K. *Program TB-LMTOASA 4.7 (tight binding-linear muffin tin orbital-atomic sphere approximation)*.
(33) Andersen, O. K. *Phys. Rev. B.* **1975**, *12*, 3060. Andersen, O. K.; Jepsen, O. *Phys. Rev. Lett.* **1984**, *53*, 2571.
(34) Savin, A.; Becke, A. D.; Flad, J.; Nesper, R.; Preuss, H.; von Schnering, H. G. *Angew. Chem.* **1991**, *103*, 421; *Angew. Chem., Int. Ed. Engl.* **1991**, *30*, 789.
(35) Barth, U.; Hedin, L. *J. Phys. C* **1972**, *5*, 1629.
(36) Pauling, L. *Die Natur der chemischen Bindung*; Verlag Chemie: GmbH., Weinheim/Bergstrasse, 1973.
(37) Further details on the crystal structures may be obtained from the Fachinformationszentrum Karlsruhe, Gesellschaft für wissenschaftlich-technische Information mbH, D-76344 Eggenstein-Leopoldshafen upon quoting the numbers CSD-405290 ($La_4I_5B_4$), CSD-405291 ($La_4Br_5B_4$), CSD-406548 ($Gd_4I_5B_4$), CSD-405294 ($La_4I_5B_2C$), and names of the authors and the journal citation.